Microchimica Acta 185 (2018): 334

DOI: https://doi.org/10.1007/s00604-018-2793-7

Synergistic effect of MoS_2 and diamond nanoparticles in electrochemical sensors : determination of an anticonvulsant drug

María Dolores Petit-Domínguez[a], Carmen Quintana[a], Luis Vázquez[b], María del Pozo[a], Isabel Cuadrado[c], Ana María Parra-Alfambra[a], Elena Casero[a]

[a]*Departamento de Química Analítica y Análisis Instrumental. Facultad de Ciencias. c/ Francisco Tomás y Valiente, Nº7. Campus de Excelencia de la Universidad Autónoma de Madrid. 28049 Madrid. Spain*

[b]*ESISNA group, Materials Science Factory, Instituto de Ciencia de Materiales de Madrid (CSIC). c/ Sor Juana Inés de la Cruz Nº3. Campus de Excelencia de la Universidad Autónoma de Madrid. 28049 Madrid. Spain*

[c]*Departamento de Química Inorgánica. Facultad de Ciencias. c/ Francisco Tomás y Valiente, Nº7. Campus de Excelencia de la Universidad Autónoma de Madrid. 28049 Madrid. Spain*

Abstract

We have developed an electrochemical sensor based on the employment of two new emerging nanomaterials: diamond nanoparticles (DNP) and molybdenum disulfide (MoS_2). The sensor was applied to the determination of an anticonvulsant, valproic acid, previously derivatized with a ferrocene group. MoS_2 platelets were obtained by an exfoliation method and DNP were directly dispersed in water and subsequently employed for glassy carbon (GC) electrodes modification. The sensor response was optimized in terms of both the solvent employed for dispersing the MoS_2 nanomaterial and the method for GC electrode modification. The better response was obtained for sensors based on a first layer of MoS_2 dispersed in ethanol:water and a second DNP layer. The different steps of the sensor construction were characterized by atomic force microscopy (AFM) and electrochemical impedance spectroscopy (EIS). In order to evaluate the synergetic effect of DNP and MoS_2, the differential pulse voltammetry (DPV) sensor response (measured at +0.18 V) was compared with that obtained, at the same potential, for sensors incorporating only one of the nanomateriales (DNP or MoS_2). Results demonstrated that the formation of a hybrid MoS_2-DNP structure clearly enhances the performance of the sensor. The sensor containing both nanomaterials exhibits a response with high sensitivity (0.74 A M^{-1}), and good detection limit and reproducibility (0.27 μM and 8%, respectively). Moreover, after 45 days the sensor retains the 99% of the initial response, showing excellent storage stability.

Keywords: molybdenum disulfide, diamond nanoparticles, valproic acid, electrochemical sensor, atomic force microscopy (AFM), electrochemical impedance spectroscopy (EIS), differential pulse voltammetry (DPV).

Introduction

Molybdenum disulfide, a member of the transition metal dichalcogenides (TMDs) family, has attracted a great interest. These emerging 2D nanomaterials, analogous to graphene, present unique mechanical, electrical, thermal and optical properties, opening up a challenging new research field [1-3].

MoS_2 nanosheets result from stacking units, formed by three atomic sulfur-molybdenum-sulfur (S-Mo-S) layers, through van der Waals interactions. In this sandwich structure, Mo atoms are coordinated in a trigonal prismatic geometry to six S atoms. There are different methods to obtain MoS_2 nanosheets based on top-down or bottom-up approaches [2]. Top-down strategies consist in breaking down bulk MoS_2 into thin layers, for example by liquid exfoliation [4-6] or by intercalating ions [7] into the weakly staked layers in order to expand them. Conversely, the bottom-up strategies lie on the synthesis of MoS_2 from building blocks such as molybdenum metal salts and organic compounds containing sulfur [8,9]. One of the most commonly employed bottom-up technique is the chemical vapor deposition [10].

MoS_2 has found its main applications in optoelectronics, generation and storage of energy i.e., supercapacitors and batteries [11-14]. In addition, the possibility of employing this nanomaterial for chemical sensing and biosensing is also attracting an increasing attention [15-19]. However, efforts devoted to employ this nanomaterial for sensing, has revealed some drawbacks. In particular, for electrochemical sensor applications, the inert nature of the basal planes, the limited number of edge sites and the low conductivity of MoS_2 nanosheets represent important disadvantages [20]. To overcome limitations and improve the activity of the MoS_2 nanosheets, an interesting strategy is related to generate hybrid structures formed by MoS_2 and conductive materials [15,16,20]. Among others, hybrids formed by MoS_2 and metal nanoparticles

[21,22], graphene [23,24], carbon nanotubes [25] or conducting polymers [26-28] have been developed and employed as sensing platforms to detect several compounds such as eugenol, glucose and dopamine [29-31].

On the other hand, diamond nanoparticles (DNP), has also gained attention as a promising nanomaterial for electrochemical sensing applications [32-34]. In particular, it presents several advantages compared to other carbon nanomaterials such as its noncytotoxic nature, good biocompatibility and low-cost.

Keeping in mind the excellent individual properties of both nanomaterials, the aim of the present work is to prove that their combination can offer new opportunities to develop electrochemical sensors with improved performances. As a proof of concept, we have evaluated the potential synergetic effect of MoS_2/DNP for the determination of valproic acid, previously derivatized with a ferrocene group (VA-Fc), to render it electroactive.

Valproic acid (VA) is an anticonvulsant employed to treat some disorders such as epilepsy, bipolar disorders and migraine headaches. Drug monitoring is important since VA displays therapeutic efficiency for plasma concentrations in the range 50-100 ppm, but can induce toxicity for higher concentrations. Analytical techniques reported in the literature for VA determination include high liquid performance chromatography (HPLC) with different detection systems, gas chromatography coupled with mass spectrometry (GC-MS), capillary electrophoresis and immunological assay, among others [35-47]. Most of these techniques usually involve a previous derivatization step in order to render the analyte suitable for detection. For example, techniques employing UV or fluorescence detection require derivatization, due to the absence of a strong chromophore or fluorophore in VA molecule. In the case of electrochemical detection, derivatization with a suitable redox group is also needed.

In the present work, we have modified for the first time a GC electrode with MoS_2 and DNP in order to develop an electrochemical sensor. The resulting device has been characterized by atomic force microscopy (AFM) and electrochemical impedance spectroscopy (EIS). AFM allows us to determine the lateral dimensions and thickness of the MoS_2 sheets, as well as the morphology of the sensing surface (MoS_2/DNP). EIS measurements allow evaluating the resistance charge transfer (R_{CT}) of MoS_2, DNP and MoS_2/DNP modified GC surfaces. The applicability of the sensor was tested for valproic acid determination (previously derivatized with a ferrocene group) in real serum samples.

Experimental Section

Materials

Diamond nanoparticles (DNP) were obtained from SkySpring Nanomaterials (Product 0512HZ, nominal diameter 4-15 nm, www.ssnano.com), Inc (Houston, Tx). Molybdenum disulfide (99%), N-methyl pyrrolidone (NMP), dimethylformamide (DMF), ethanol (EtOH), isopropyl alcohol (IPA), methanol, dichloromethane, triethylamine, dopamine, ascorbic acid, epinephrine, lithium tetrahydridoaluminate, potassium ferrocyanide, potassium ferricyanide, potassium cyanide, and potassium chloride were obtained from Aldrich Chemical Co (www.sigmaaldrich.com). 2,2-di-n-propylacetic acid and *N*,*N*,*N*-trimethylferrocenylmethyl-amonium iodide were obtained from Alfa Aesar (www.alfa.com/es). Sodium phosphate (www.merck.com) was employed for the preparation of buffers. Water was purified with a Millipore Milli-Q-System (www.millipore.com). All solutions were prepared just prior to use.

Experimental techniques

The AFM measurements were performed in air with Nanoscope IIIa (Veeco, www.veeco.com) and Agilent 5500 (Agilent, www.agilent.com) systems. The images were taken in the dynamic mode using silicon cantilevers (Bruker, www.bruker.com) with a nominal force constant of 40 N/m and a nominal radius of 8 nm. First, large areas (around 100 μm^2) were scanned in order to locate the MoS_2 flakes, which were then imaged at higher resolution. The images, 1024 x 1024 pixels, were taken with different cantilevers in order to ensure that the imaged structures were not due to tip artefacts. Also, eventually imaging under liquid conditions was performed in order to discard artefacts coming from remaining water used in the sample preparation. Supports used were Si substrates from University Wafer (www.universitywafer.com, USA).

Impedance and voltammetric studies were carried out with an Ecochemie Autolab PGSTAT302 N system (Utrecht, The Netherlands, www.ecochemie.nl) in a cell with a working GC electrode (3 mm internal diameter) and a platinum wire as counter electrode (www.metrohm.com). All potentials were reported with respect to a Ag/AgCl reference electrode. DPV measurements were carried out in a 0.1 M phosphate buffer (pH = 7) containing VA-Fc, with the following conditions: range potential from -50 mV to 450 mV, scan rate 10 mVs^{-1}, pulse amplitude 60 mV and step potential 1 mV. EIS experiments were performed in a 0.1 M phosphate buffer (pH = 7), containing 10 mM $K_3Fe(CN)_6$/ $K_4Fe(CN)_6$. A sinusoidal potential modulation of ±10 mV amplitude in the 10^5 Hz-10^{-2} Hz frequency range, spaced logarithmically (120 per 8 decades), was superimposed onto the formal potential of the redox couple, $[Fe(CN)_6]^{3-/4-}$.

HPLC measurements were performed with a Jasco Analytica PU-1580 high pressure pumping system, equipped with Rheodyne Model 7125 injector with a 20 µL loop and a

Kromasil C18 column (150 x 4.6 mm; 5 μm; Scharlau). A Perkin Elmer 785A UV/VIS was employed as detector at λ= 260 nm.

Functionalization of valproic acid with aminoethyl-substituted ferrocene

Organometallic compound Fe{[(η^5-C_5H_4)$(CH_2)_2$NHC(O)CH$(CH_2CH_2CH_3)_2$](η^5-C_5H_5)} (VA-Fc) was synthesized by direct amide coupling of equimolar amounts of β-aminoethylferrocene Fe{(η^5-$C_5H_4(CH_2)_2NH_2$)(η^5-C_5H_5)} (500 mg, 2.18 mmol) with 2,2-di-n-propylacetic acid, in dry CH_2Cl_2, in the presence of triethylamine. The solution was concentrated and the solid formed was separated by filtration and dried under vacuum to afford the desired compound VA-Fc which was isolated as a yellow-orange solid (yield: 53%). Data obtained from ^{1}H NMR, IR and MS (FB^+) confirm that VA-Fc has been successfully synthesized (data not shown).

Compound Fe{(η^5-$C_5H_4(CH_2)_2NH_2$)(η^5-C_5H_5)} [48, 49] was selected as starting metallocene since the reactive NH_2 functionality is separated from the cyclopentadienyl ring by a two methylene flexible bridge. This fact is of importance because it minimizes steric and electronic effects of the organometallic ferrocene moiety. The use of a β-functionalized metallocene, in addition, avoids the instability of α-functional ferrocene derivatives resulting from the stability of the α-ferrocenyl carbonium ion.

Concerning monofunctionalized ferrocene Fe{(η^5-$C_5H_4(CH_2)_2NH_2$)(η^5-C_5H_5)} this compound was prepared in two steps from *N*,*N*,*N*-trimethylferrocenylmethyl-amonium iodide as starting material by adapting the literature procedures [50]. Firstly, [(η^5-C_5H_5)Fe{η^5-C_5H_4)$CH_2N(CH_3)_3$}]I was reacted with potassium cyanide thus resulting 1-cyanomethylferrrocene which was isolated as a yellow crystalline solid in 63% yield. The cyanomethylferrocene was converted into β-aminoethylferrocene by reduction with $LiAlH_4$ followed by treatment with aqueous sodium hydroxide. After aqueous workup

and distillation in vacuum, primary amine Fe{(η^5-$C_5H_4(CH_2)_2NH_2$)(η^5-C_5H_5)} was obtained as an amber-brown oil in 66% yield.

VA-Fc was dissolved in methanol, giving rise to a 2.2 10^{-3} M VA-Fc stock solution. Working solutions were prepared by dilution of the stock solution in phosphate buffer 0.1 M pH=7.0.

Synthesis of MoS_2 platelets

MoS_2 nano-sized powders were employed as starting materials to obtain MoS_2 atomic layers following a liquid exfoliation strategy [4], with some modifications. The solvents selected as exfoliation mediums were NMP, DMF, EtOH/water (45:55) and IPA/water (45:55). Briefly, 75 mg of the commercial MoS_2 powder was mixed with 10.0 mL of the corresponding solvent. After sonication of each dispersion for 2 hours, it was kept at 4 ºC during 24 hours and then centrifuged (1500 rpm, 45 minutes). The supernatant was collected and subsequently employed for electrode modification.

Preparation of the samples for AFM measurements

Samples for AFM measurements were prepared by modifying Si surfaces as follows: i) placing 6 µL of MoS_2 exfoliated in EtOH/water, ii) leaving air-dry and iii) depositing 6 µL of DNP dispersed in water (1 mg mL^{-1}). An additional sample was prepared in the same way but employing DNP diluted 1:1000 with water (1 µg mL^{-1}).

Preparation of the electrochemical sensors. Evaluation of the response.

GC electrodes were polished with 1 µm diamond paste (Buehler) and rinsed with water. Subsequently, four different sensors were obtained by modifying these GC electrodes as follows: i) placing 6 µL of MoS_2 exfoliated in NMP, DMF, EtOH/water or

IPA/water solvent, ii) leaving air-dry, iii) depositing 6 µL of DNP dispersed in water (1 mg mL^{-1}) and air-dry again. For comparison, four other electrochemical sensors consisting in a first layer of DNP and a second layer of MoS_2 (exfoliated in NMP, DMF, EtOH/water or IPA/water) were also prepared following the same procedure but inverting the order of MoS_2 and DNP deposition.

Sensors containing only MoS_2 or DNP were obtained by modifying the GC electrode with 6 µL of the corresponding nanomaterial and leaving air-dry it.

The sensor response was evaluated as follows: the electrodes, modified as described above, were introduced into an electrochemical cell containing 3.5 µM of VA-Fc in 0.1 M phosphate buffer (pH = 7) and the differential pulse voltammograms were obtained (see DPV conditions in the experimental techniques section). The calibration curve was obtained: i) recording DPVs for different VA-Fc concentrations in the range potential from -50 mV to 450 mV, ii) plotting the intensity current obtained at +0.18 V towards the corresponding VA-Fc concentration.

Evaluation of the method: VA-Fc analysis in serum samples.

Human blood was centrifuged at 4 ºC for 10 min at 2500 rpm. The serum was then separated with a syringe and stored at 4 ºC prior to analysis. Samples were diluted 1:100 with phosphate buffer (pH 7) and spiked with five different VA-Fc concentrations (from 1.4 10^{-6} M to 5.5 10^{-6} M). The determination was carried out by the DPV method in order to calculate the recoveries.

HPLC-UV measurements were performed for comparison. Chromatograms were obtained at a flow rate of 1.0 mL min^{-1}, employing EtOH/NaH_2PO_4 0.01 M (60:40, v/v) as mobile phase, pH 6. A wavelength of 260 nm was employed for detection. Serum samples were diluted 1:100 in mobile phase and spiked to obtain final VA-Fc

concentrations of 1.0 10^{-5}, 2.5 10^{-5} and 5.0 10^{-5} M. Samples were filtered through a 0.45 μm pore size nylon filter.

Results and discussion

We have developed an electrochemical sensor by combining two nanomaterials, DNP and MoS_2, which are attracting an emerging attention in the sensors field. As mentioned in the introduction, several (bio)sensors have been developed using one of these two nanomaterials, leading to improved performances. Thus, their excellent individual properties suggest the possibility of giving rise to a synergistic effect when employed together. In particular, the presence of DNP can overcome one of the main drawbacks of employing MoS_2 in electrochemical sensors, related to its low conductivity. Until now, hybrids formed by MoS_2 and different nanomaterials such as graphene or carbon nanotubes have been assayed as sensor platforms, but DNP have not been tested for this goal.

Optimization of the sensor construction

Following the procedure described in the experimental section, we have exfoliated molybdenum disulfide by sonication in four different solvents to produce stable MoS_2 dispersions sheets. In order to evaluate the suitability of a given solvent, we have obtained the response of four different sensors fabricated by modifying GC electrodes with DNP and MoS_2 previously exfoliated in NMP, DMF, EtOH/H_2O and IPA/H_2O, respectively. The differential pulse voltammograms, displayed in Figure 1, are obtained in a 0.1 M phosphate buffer pH=7.0, containing 3.5 μM of VA-Fc. Although a well-defined oxidation peak, corresponding to VA-Fc, is observed for all cases, the response is clearly better when EtOH/H_2O is employed as solvent. In particular, the peak current

measured at a potential of +0.18 V is approximately three times higher in comparison to the current obtained for the rest of solvents.

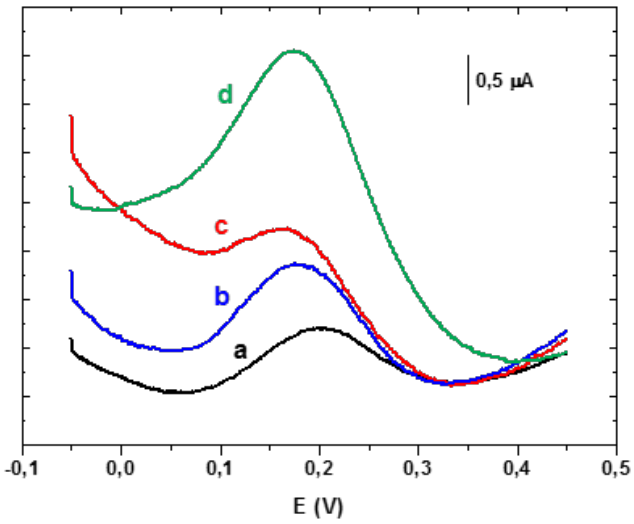

Figure 1. DPV response of GC electrodes modified with DNP and MoS_2 in a 0.1 M phosphate buffer pH=7.0, containing 3.5 µM of VA-Fc. MoS_2 employed for the sensors fabrication had been previously exfoliated employing as solvent: (a) NMP, (b) DMF, (c) IPA/water and (d) EtOH/water. DPV conditions: range potential from -50 mV to 450 mV, scan rate 10 mV s^{-1}, pulse amplitude 60 mV and step potential 1 mV.

Once $EtOH/H_2O$ was selected as solvent, we proceeded to optimize the modification procedure. In order to do this, two different sensor configurations have been compared. The first one corresponds to that described until now, a first layer of MoS_2 in direct contact with the GC surface, and a second layer of DNP in contact with the medium. The response of this sensor ($GC/MoS_2/DNP$) has been previously shown (Figure 1, curve d). The second configuration is just the opposite, an inner DNP layer in contact with the electrode and an outer MoS_2 layer. The response obtained with this configuration ($GC/DNP/MoS_2$) is similar or even higher (data not shown), than that corresponding to $GC/MoS_2/DNP$. However, this sensor arrangement was discarded due to its poor stability. In particular, the DPV measured after 3 days is similar to that obtained for the GC/DNP system, suggesting that the MoS_2 layer is partially lost when

it is directly exposed to the medium. When this layer is protected by DNP the stability sensor is highly improved as it will be discussed later.

Finally, some experimental conditions, such as pH, electrolyte and pulse amplitude in DPV measurements were optimized. In particular, the response of a GC/MoS_2/DNP electrode was obtained in the following electrolytes, containing 3.5 μM of VA-Fc: acetate buffer at pH=4.0, phosphate buffer at pH=7.0 and borate buffer at pH=10.0. Concerning pulse amplitude, values in the range 10-80 mV were assayed. The best results were obtained for phosphate buffer at pH 7.0 and a pulse amplitude of 60 mV.

Morphological sensor characterization: AFM measurements

The different steps of the sensor construction were characterized by atomic force microscopy (AFM). Figure 2A shows a 5 x 5 μm^2 image in which several MoS_2 platelets can be observed. They have a height in the 4-6 nm range. Their size varies from few nm^2 to areas above 1 μm^2. This sample in fact corresponds to a MoS_2 sample on which DNP (from a diluted stock, 1 μg mL^{-1}) were deposited (see the experimental section). It can be distinguished how these DNP are deposited, mainly as aggregates, on top of the large MoS_2 platelets. When the background of the image is inspected in detail, a small structure can be discerned. When this zone is imaged at higher resolution, images as that of Figure 2B are obtained. Here, small plateaus are observed with relatively jagged perimeters and lateral sizes below 200 nm. From the height distribution of the image (Figure 2C) it is clearly obtained that the average measured height of these flakes is close to 0.8 nm, i.e., very close (within the error bar) to that of a MoS_2 monolayer. It should be noted that, in this height histogram, we have taken the zero height value at the lowest point of the whole image and not at the average height of the flat background (which is located in the histogram at 0.6 nm). Thus, the MoS_2

thickness is the height difference, along the x-axis of the histogram, between both peaks. In Figure 2D is displayed an image taken on a sample prepared by using the same concentration of both the DNP and MoS_2 employed in the samples characterized electrochemically. In particular, now, the DNP number is considerably higher than in Figure 2A since a DNP stock of 1 mg mL^{-1} was employed for modification. Notwithstanding, once more rather flat platelets are imaged with heights in the 3-5 nm range. However, most of them are almost totally covered by DNP (for instance the large one at the top left corner of the image) while others (as that at the top right corner and the one close to the center of the image) have only some DNP on their surface. The DNP height is in the 5-15 nm range. Interestingly, they tend to aggregate on these partially DNP-covered MoS_2 flakes mainly at their perimeter, i.e., at the steps. In contrast with Figure 2A, now the DNP are also found on the substrate, outside the MoS_2 flakes, which is likely due to their high amount. Finally, in Figure 2E is displayed a zoom of one of these partially DNP-covered MoS_2 flakes. This flake has a thickness close to 5.5 nm and the DNP on top are 8-15 nm high. At given spots, mostly at the perimeter of the flake, aggregation of DNP is observed.

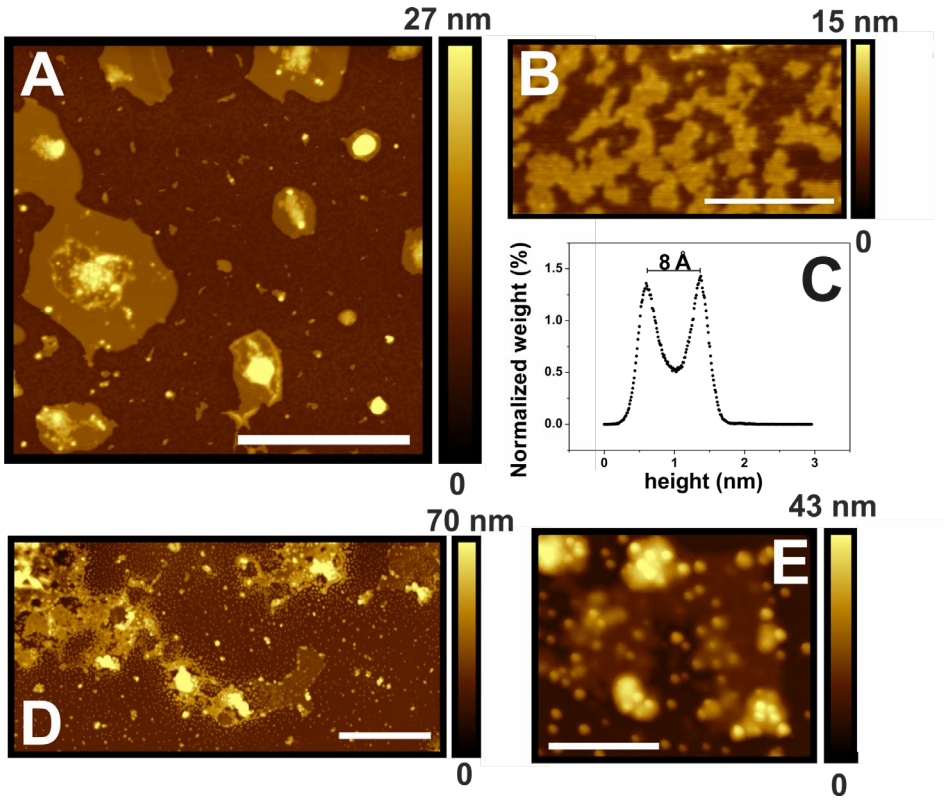

Figure 2. (A) AFM image of SiO_2 substrates modified with MoS_2 and DNP for a low DNP concentration. (B) High resolution image of the flat background revealing the presence of small MoS_2 flakes. Its corresponding height distribution is shown in (C). Note that we have taken the zero height value at the lowest point of the whole image. (D) AFM image of SiO_2 substrates modified with MoS_2 and DNP nanostructures for a high DNP concentration. (E) Detail of a MoS_2 flake partially covered by DNP. The horizontal bars indicate (A) 2 µm, (B) 500 nm, (D) 3 µm and (E) 500 nm, respectively. Note that (B) and (E) are not zoomed regions of (A) and (D), respectively but rather higher resolution images taken on similar zones of the sample.

Evaluation of the MoS_2 and DNP synergetic effect in electrochemical sensing

In order to evaluate the synergetic effect of both nanomaterials, the response of the GC/MoS_2/DNP sensor was compared to that of sensors containing only one of the nanostructures, DNP or MoS_2. Figure 3 shows the differential pulse voltammograms of bare GC, GC/MoS_2, GC/DNP and GC/MoS_2/DNP systems. The oxidation peak, corresponding to VA-Fc, is observed for all cases, but its intensity current (measured at +0.18 V) depends on the specific electrode modification. Bare GC electrodes (curve a) and MoS_2-based sensors (curve b) lead to a similar intensity current response, lower than that corresponding to DNP-based ones (curve c). As displayed in curve d, the

simultaneous presence of MoS_2 and DNP gives rise to an intensity current response that is nine and five times higher than that of GC/MoS_2 and GC/DNP, respectively. This result indicates that employing MoS_2 and DNP together as sensing elements allows the development of electrochemical sensors with an enhanced performance. Although we have only tested it in the particular case of VA-Fc determination, this promising starting point suggests the possibility of a broad applicability for determination of other analytes.

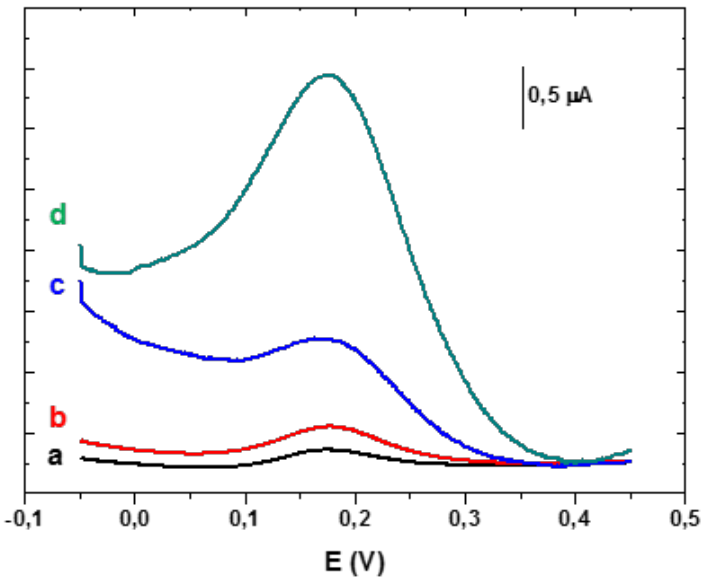

Figure 3. DPV response of (a) bare GC, (b) GC/MoS_2, (c) GC/DNP and (d) GC/MoS_2/DNP electrodes in a 0.1 M phosphate buffer pH=7.0, containing 3.5 µM of VA-Fc. MoS_2 employed for the sensor fabrication has been previously exfoliated employing as solvent EtOH/water. DPV conditions: range potential from -50 mV to 450 mV, scan rate 10 mV s^{-1}, pulse amplitude 60 mV and step potential 1 mV.

The improved response obtained for the sensor containing both nanomaterials is likely due to an increase of both the effective surface area of the electrode and the efficiency in the charge transfer caused by the concomitant presence of MoS_2 and DNP. In order to confirm the latter point, the interfacial properties of bare and modified glassy carbon electrodes were studied by EIS. Figure 4 displays the Nyquist diagrams for GC,

GC/MoS_2, GC/DNP and GC/MoS_2/DNP systems. The semicircles correspond to the charge transfer resistance (R_{CT}) limiting process that is associated with the surface/electrolyte interface. The linear part corresponds to the diffusion-controlled process.

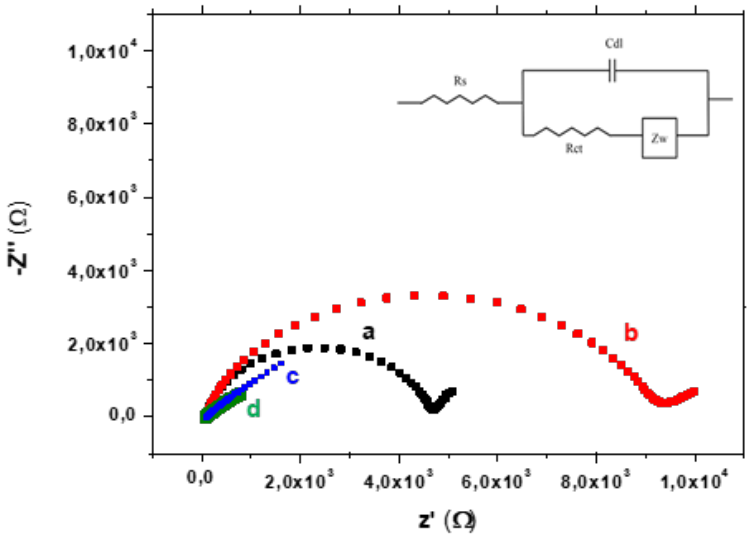

Figure 4. Nyquist plots of (a) bare GC, (b) GC/MoS_2, (c) GC/DNP and (d) GC/MoS_2/DNP electrodes obtained in a 0.1 M phosphate buffer (pH = 7) containing 10 mM [Fe $(CN)_6$] $^{3-/4-}$ by applying a sinusoidal potential modulation with amplitude of ±10 mV over the frequency range 10^5 Hz-10^{-2} Hz. Inset: Randles electrical equivalent circuit.

The impedance diagrams were fitted considering the Randles electrical equivalent circuit, shown in the inset of Figure 4, where Rs, R_{CT}, C_{dl} and Z_W are the electrolyte resistance, the charge transfer resistance, the double layer capacitante and the Warburg impedance, respectively. From the fit, R_{CT} values of 4536.4 Ω and 9000 Ω were obtained for GC and GC/MoS_2, respectively. Upon modification of the GC surface with MoS_2 (curve b), it results an increase of the charge transfer resistance value with respect to the bare GC electrode (curve a). This fact suggests that MoS_2 hinders the electron transfer between the redox probe, [Fe $(CN)_6$]$^{3-/4-}$and the glassy carbon electrode. In contrast, for both the GC/DNP and the GC/MoS_2/DNP systems, just a straight line with

a slope close to 1 (0.94 and 0.93, respectively) is obtained (curves c and d). Therefore, the presence of DNP in the surface clearly improves the charge transfer, being a diffusion-limited transport process observed. This behavior confirms that MoS_2/DNP hybrid structures improve the electron transfer with respect to a MoS_2 modified surface, rendering it very attractive for electrochemical sensors development.

On the other hand, the electrochemical surface area was determined by recording five consecutive cyclic voltamogramms at 50 mVs^{-1} with the different modified electrodes in a KCl 1M solution containing 5.0 mM $K_4[Fe(CN)_6]$ / $K_3[Fe(CN)_6]$. The mean measured peak current (I_p) is related with the electrochemical surface area (A) through the Randles-Sevick equation:

$$Ip_a = (2.69 \times 10^5)\, n^{3/2}\, A\, D^{½}\, v^{½}\, C$$

where v is the scan rate, n the number of electrons, D the diffusion coefficient (6.5 10^{-6} cm^2 s^{-1} at 20 ºC [51]) and C the concentration of the redox compound. Electrochemical surface areas of (0.065 ± 0.004) cm^2, (0.0784 ± 0.0005) cm^2 and (0.0896 ± 0.0003) cm^2 were obtained for GC, GC/DNP and GC/MoS_2/DNP electrodes, respectively. These values confirm that the presence of both nanomaterials results in a considerable increase of the effective area.

Response of the GC/MoS_2/DNP sensor towards increasing VA-Fc concentration

Once the synergetic effect of MoS_2 and DNP has been assessed, DPVs of GC/MoS_2/DNP at increasing VA-Fc concentration were recorded (Figure S1). The current measured at a potential of +0.18 V was plotted as a function of the VA-Fc concentration in solution (data not shown), being linear in the range from 9.0 10^{-7} M to 5.5 10^{-6} M, according to the following equation I (A) = 7 10^{-8} (±3 10^{-8}) + 0.74 (±0.01) C (M), with a correlation coefficient of 0.990. The sensitivity, calculated as the slope of

390 the calibration curve, was 0.74 A M^{-1} (8.26 A M^{-1} cm^{-2}, when normalized to the
391 electrochemical area). The detection and quantification limits, obtained as the ratio
392 between three and ten times the standard deviation of the blank signal and the
393 sensitivity, were 2.7 10^{-7} M and 9.0 10^{-7} M, respectively. As can be observed in Table
394 S1, the detection limit is similar or even better than those obtained by others methods
395 commonly employed for VA determination [35-47]. Note that some of the analytical
396 techniques reported in the literature require the derivatization of VA. For example, for
397 optical detection, derivatization with a chromophore/fluorophore is usually performed
398 in an attempt of improving sensitivity, given the poor valproic acid UV absorption
399 capacity. In our case, for electrochemical detection, derivatization with a suitable redox
400 group is also needed, in order to obtain a redox response at around +0.2 V, which
401 minimize the potential interferents. From the point of view of derivatization, our
402 method does not represent an improvement with respect to the other techniques usually
403 employed, such as HPLC or GC-MS, but it is less expensive and less time consuming,
404 requiring also less sophisticated equipments.

405 Finally, reproducibility and stability were evaluated. Reproducibility was estimated
406 by measuring 2.2 10^{-6} M of VA-Fc with parallel GC/MoS_2/DNP sensors. A relative
407 standard deviation value (RSD) of 8% is obtained for five different measurements
408 (n=5). Concerning operational stability, a RSD value of 6% was obtained for 50
409 consecutive measurements with the same GC/MoS_2/DNP sensor. Storage stability was
410 also studied by recording DPVs of a GC/MoS_2/DNP sensor every 15 days. The sensor
411 was kept at 4 ºC between measurements. Even after 45 days, 99 % of the original
412 response was retained, indicating an excellent stability.

413 In order to evaluate the selectivity, the influence of several potential interferences on
414 the sensor response was studied. In this sense, we have obtained the sensor response

before and after adding increasing amounts of dopamine, ascorbic acid and epinephrine to a solution containing 1.0 10^{-6} M of VA-Fc. It was considered that each compound interferes at a concentration level enough to produce a variation of 10% in the initial response. According to this, the presence of epinephrine, ascorbic acid and dopamine in the sample interferes for concentrations of 5.0 10^{-6} M, 2.5 10^{-6} M, and 1.8 10^{-6} M, respectively. Note that the interference concentration level for all the compounds assayed ranges from 2 to 5 times higher than the VA-Fc concentration in solution.

Analytical application in real samples: determination of VA-Fc in serum

The applicability of the sensor was tested for VA-Fc determination in serum samples. As mentioned in the experimental section, human blood was centrifuged at 4 ºC for 10 min at 2500 rpm. The serum was then separated with a syringe and stored at 4 ºC prior to analysis. Samples were diluted 1:100 with phosphate buffer pH 7.0 and spiked with five different VA-Fc concentrations (from 1.4 10^{-6} M to 5.5 10^{-6} M). Dilution 1:100 allows obtaining a final concentration that both corresponds with possible physiological concentrations and fits in the linear range of the sensors. The VA-Fc determination was carried out by the DPV method (see experimental section). The recoveries, obtained for each VA-Fc concentration essayed, are summarized in Table 1. The recoveries were from 96% to 111%, indicating that the sensor can be successfully used to detect VA-Fc.

$[VA\text{-}Fc]_{added}$ (M)	$[VA\text{-}Fc]_{found}$ (M)	Recovery (%)
1.4 10^{-6}	1.6 10^{-6}	111
2.2 10^{-6}	2.3 10^{-6}	106
3.9 10^{-6}	4.1 10^{-6}	106
5.5 10^{-6}	5.3 10^{-6}	96

Table 1. Recoveries of VA-Fc from spiked serum samples

For evaluating the feasibility of the electrochemical method, serum samples were also analyzed by high-performance liquid chromatography (HPLC-UV) technique. Chromatographic conditions were selected according to reference 52 (see experimental section). Under these conditions, retention time of VA-Fc was 13.3 minutes. From the analysis of VA-Fc solutions of increasing concentrations, a good linearity of the calibration graph is obtained: A=-1854 (±7) + 179 (±8) 10^{7} C (M); r=0.999. As described in experimental section, three different samples (spiked to obtain final VA-Fc concentrations of 1.0 10^{-5}, 2.5 10^{-5} and 5.0 10^{-5} M) were injected in the chromatographic system. Recoveries of 93%, 84% and 81%, respectively were obtained, demonstrating that similar recoveries are obtained by both methods.

4. Conclusions

In the present study, we have developed the first electrochemical sensor based on the combined employment of MoS_2 nanosheets and DNP as sensing elements and we have proved its applicability for determination of valproic acid previously derivatized with a ferrocene group. The best results were obtained for sensors developed employing MoS_2 dispersed in EtOH/water with a configuration consisting in a first layer of MoS_2 and a second layer of DNP. Concerning the morphology of the sensor surface, rather flat MoS_2 platelets are observed by AFM, being most of them almost totally covered by DNP. The presence of DNP significantly decreases the resistance charge transfer of the sensor surface compared to MoS_2. We prove that the combination of MoS_2 and DNP led to sensors with an enhanced analytical performance towards the oxidation of VA-Fc in comparison with sensors containing only one of the nanomaterials. Since an important synergistic effect takes place, the combination of these both emergent nanomaterials can offer new opportunities to develop electrochemical sensors with improved performances

for detection of different analytes, suggesting the possibility of a broad applicability. In our case, since valproic acid is not electroactive, its derivatization with a redox group is needed as previous step.

Acknowledgments

The authors would like to thank Ministerio de Economía, Industria y Competitividad (MAT2017-85089-C2-1-R, MAT2017-85089-C2-2-R) and the Comunidad Autónoma de Madrid (S2013/MIT-3029, NANOAVANSENS) for financial support.

REFERENCES

1. Gupta A, Sakthivel T, Seal S (2015) Recent development in 2D materials beyond graphene. Prog Mater Sci 73:44-126
2. Huang X, Zeng Z, Zhang H (2013) Metal dichalcogenide nanosheets: preparation, properties and applications. Chem Soc Rev 42 (5):1934-1946
3. Mas-Ballesté R, Gómez-Navarro C, Gómez-Herrero J, Zamora F (2011) 2D materials: to graphene and beyond. Nanoscale 3 (1):20-30
4. Coleman JN, Lotya M, O'Neill A, Bergin SD, King PJ, Khan U, Young K, Gaucher A, De S, Smith RJ, Shvets IV, Arora SK, Stanton G, Kim HY, Lee K, Kim GT, Duesberg GS, Hallam T, Boland JJ, Wang JJ, Donegan JF, Grunlan JC, Moriarty G, Shmeliov A, Nicholls RJ, Perkins JM, Grieveson EM, Theuwissen K, McComb DW, Nellist PD, Nicolosi V (2011) Two-dimensional nanosheets produced by liquid exfoliation of layered materials. Science 331 (6017):568-571
5. Cunningham G, Lotya M, Cucinotta CS, Sanvito S, Bergin SD, Menzel R, Shaffer MSP, Coleman JN (2012) Solvent exfoliation of transition metal dichalcogenides: dispersability of exfoliated nanosheets varies only weakly between compounds ACS Nano 6 (4):3468-3480
6. Smith RJ, King PJ, Lotya M, Wirtz C, Khan U, De S, O'Neill A, Duesberg GS, Grunlan JC, Moriarty G, Chen J, Wang J, Minett AI, Nicolosi V, Coleman JN (2011) Large-scale exfoliation of inorganic layered compounds in aqueous surfactant solutions. Adv Mater 23 (34):3944-3948
7. Zeng Z, Sun T, Zhu J, Huang X, Yin Z, Lu G, Fan Z, Yan Q, Hng HH, Zhang H (2012) An effective method for the fabrication of few-layer-thick inorganic nanosheets. Angew Chem 51 (36):9052-9056
8. Liu BK-k, Zhang W, Lee Y-h, Lin Y-c (2012) Growth of large-area and highly crystalline MoS_2 thin layers on insulating substrates. Nano Lett 2:1-9
9. Ye L, Xu H, Zhang D, Chen S (2014) Synthesis of bilayer MoS_2 nanosheets by a facile hydrothermal method and their methyl orange adsorption capacity. Mater Res Bull 55 (2):221-228
10. Zhan Y, Liu Z, Najmaei S, Ajayan PM, Lou J (2012) Large-area vapor-phase growth and characterization of MoS_2 atomic layers on a SiO_2 substrate. Small 8 (7):966-971
11. Gong Y, Yang S, Zhan L, Ma L, Vajtai R, Ajayan PM (2014) A bottom-up approach to build 3D architectures from nanosheets for superior lithium storage. Adv Funct Mater 24 (1):125-130
12. Kappera R, Voiry D, Yalcin SE, Branch B, Gupta G, Mohite AD, Chhowalla M (2014) Phase-engineered low-resistance contacts for ultrathin MoS_2 transistors. Nat mater 13 (August):1-15
13. Lukowski MA, Daniel AS, Meng F, Forticaux A, Li L, Jin S (2013) Enhanced hydrogen evolution catalysis from chemically exfoliated metallic MoS_2 nanosheets. J Am Chem Soc 135 (28):10274-10274
14. Wang X, Weng Q, Yang Y, Bando Y, Golberg D (2016) Hybrid two-dimensional materials in rechargeable battery applications and their microscopic mechanisms. Chem Soc Rev 45 (15):4042-4073
15. Huang Y, Guo J, Kang Y, Ai Y, Li CM (2015) Two dimensional atomically thin MoS_2 nanosheets and their sensing applications. Nanoscale 7 (46):19358-19376
16. Pumera M, Loo AH (2014) Layered transition-metal dichalcogenides (MoS_2 and WS_2) for sensing and biosensing. Trends Anal Chem 61:49-53
17. Shavanova K, Bakakina Y, Burkova I, Shtepliuk I, Viter R, Ubelis A, Beni V, Starodub N, Yakimova R, Khranovskyy V (2016) Application of 2D non-graphene materials and 2D oxide nanostructures for biosensing technology. Sensors 16 (2):1-23
18. Yan L, Shi H, Sui X, Deng Z, Gao L (2017) MoS_2-DNA and MoS_2 based sensors. RSC Adv 7:23573-23582
19. Zhu C, Du D, Lin Y (2015) Graphene and graphene-like 2D materials for optical biosensing and bioimaging: a review. 2D Mater 2 (3):032004-032004
20. Lv Z, Mahmood N, Tahir M, Pan L, Zhang X, Zou J-j (2016) Fabrication of zero to three dimensional nanostructured molybdenum sulfides and their electrochemical and photocatalytic applications. Nanoscale 8:18250-18269
21. Huang J, Dong Z, Li Y, Li J, Tang W, Yang H, Wang J, Bao Y, Jin J, Li R (2013) MoS_2 nanosheet functionalized with Cu nanoparticles and its application for glucose detection. Mater Res Bull 48 (11):4544-4547
22. Huang KJ, Liu YJ, Liu YM, Wang LL (2014) Molybdenum disulfide nanoflower-chitosan-Au nanoparticles composites based electrochemical sensing platform for bisphenol a determination. J Hazard Mater 276:207-215
23. Huang KJ, Wang L, Li J, Liu YM (2013) Electrochemical sensing based on layered MoS_2-graphene composites. Sens Actuators B Chem 178:671-677
24. Song H, Ni Y, Kokot S (2014) Investigations of an electrochemical platform based on the layered MoS_2-graphene and horseradish peroxidase nanocomposite for direct electrochemistry and electrocatalysis. Biosens Bioelectron 56:137-143

25. Huang KJ, Liu YJ, Wang HB, Wang YY, Liu YM (2014) Sub-femtomolar DNA detection based on layered molybdenum disulfide/multi-walled carbon nanotube composites, Au nanoparticle and enzyme multiple signal amplification. Biosens Bioelectron 55:195-202
26. Huang K-j, Zhang J-z, Liu Y-j, Wang L-l (2014) Novel electrochemical sensing platform based on molybdenum disulfide nanosheets-polyaniline composites and Au nanoparticles. Sens Actuators B Chem 194:303-310
27. Yang T, Chen M, Nan F, Chen L, Luo X, Jiao K (2015) Enhanced electropolymerization of poly(xanthurenic acid)-MoS_2 film for specific electrocatalytic detection of guanine and adenine. J Mater Chem B 3 (24):4884-4891
28. Sajedi-Moghaddam A, Saievar-Iranizad E, Pumera M (2017) Two-dimensional transition metal dichalcogenide/conducting polymer composites: synthesis and applications. Nanoscale 9 (24):8052-8065
29. Feng Q, Duan K, Ye X, Lu D, Du Y, Wang C (2014) A novel way for detection of eugenol via poly (diallyldimethylammonium chloride) functionalized graphene-MoS_2 nano-flower fabricated electrochemical sensor. Sens Actuators B Chem 192:1-8
30. Su S, Sun H, Xu F, Yuwen L, Fan C, Wang L (2014) Direct electrochemistry of glucose oxidase and a biosensor for glucose based on a glass carbon electrode modified with MoS_2 nanosheets decorated with gold nanoparticles. Microchim Acta 181 (13-14):1497-1503
31. Su S, Sun H, Xu F, Yuwen L, Wang L (2013) Highly sensitive and selective determination of dopamine in the presence of ascorbic acid using gold nanoparticles-decorated MoS_2 nanosheets modified electrode. Electroanalysis 25 (11):2523-2529
32. Briones M, Casero E, Petit-Domínguez MD, Ruiz MA, Parra-Alfambra AM, Pariente F, Lorenzo E, Vázquez L (2015) Diamond nanoparticles based biosensors for efficient glucose and lactate determination. Biosens Bioelectron 68:521-528
33. Briones M, Casero E, Vázquez L, Pariente F, Lorenzo E, Petit-Domínguez MD (2016) Diamond nanoparticles as a way to improve electron transfer in sol-gel L-lactate biosensing platforms. Anal Chim Acta 908:141-149
34. Briones M, Petit-Domínguez MD, Parra-Alfambra AM, Vázquez L, Pariente F, Lorenzo E, Casero E (2016) Electrocatalytic processes promoted by diamond nanoparticles in enzymatic biosensing devices. Bioelectrochemistry 111:93-99
35. Stephenson JB, Flater ML, Bain LT (2016) Analysis of valproic acid, salicylic acid and ibuprofen in whole blood by GC-MS. J Anal Toxicol 40:649–652
36. Dziadosz M (2017) The application of multiple analyte adduct formation in the LC–MS3 analysis of valproic acid in human serum. J Chromatogr B Anal Technol Biomed Life Sci 1040:159–161 .
37. Silva-Trujillo A, Correa-Basurto J, Romero-Castro A, et al (2015) A simple validated RP-HPLC bioanalytical method for the quantitative determination of a novel valproic acid arylamide derivative in rat hepatic microsomes. Biomed Chromatogr 29:523–528 .
38. Zhang JF, Zhang ZQ, Dong WC, et al (2014) A New Derivatization Method to Enhance Sensitivity for the Determination of Low Levels of Valproic Acid in Human Plasma. J. Chromatogr. Sci. 52:1173–1180.
39. Joo KM, Choi D, Park YH, et al (2013) A rapid and highly sensitive UPLC-MS/MS method using pre-column derivatization with 2-picolylamine for intravenous and percutaneous pharmacokinetics of valproic acid in rats. J Chromatogr B Anal Technol Biomed Life Sci 938:35–42 .
40. Chen ZJ, Wang XD, Wang HS, et al (2012) Simultaneous determination of valproic acid and 2-propyl-4-pentenoic acid for the prediction of clinical adverse effects in Chinese patients with epilepsy. Seizure 21:110–117.
41. Cheng H, Liu Z, Blum W, et al (2007) Quantification of valproic acid and its metabolite 2-propyl-4-pentenoic acid in human plasma using HPLC-MS/MS. J Chromatogr B Anal Technol Biomed Life Sci 850:206–212
42. Shahdousti P, Mohammadi A, Alizadeh N (2007) Determination of valproic acid in human serum and pharmaceutical preparations by headspace liquid-phase microextraction gas chromatography-flame ionization detection without prior derivatization. J Chromatogr B, 850: 128–133
43. Pham TTT, See HH, Morand R, et al (2012) Determination of free and total valproic acid in human plasma by capillary electrophoresis with contactless conductivity detection. J Chromatogr B Anal Technol Biomed Life Sci 907:74–78 .
44. Zabardasti A, Afrouzi H, Talemi RP (2017) A simple and sensitive methodology for voltammetric determination of valproic acid in human blood plasma samples using 3-aminopropyletriethoxy silane coated magnetic nanoparticles modified pencil graphite electrode. Mater Sci Eng C 76:425–430 .
45. Huang LS, Gunawan C, Yen YK, Chang KF (2015) Direct determination of a small-molecule drug, valproic acid, by an electrically-detected microcantilever biosensor for personalized diagnostics. Biosensors 5:37–50 .

46. Sorouraddin MH, Imani-Nabiyyi A, Najibi-Gehraz SA, Rashidi MR (2014) A new fluorimetric method for determination of valproic acid using TGA-capped CdTe quantum dots as proton sensor. J Lumin 145:253–258 .
47. Santos EMG, Araújo AN, Couto CMCM, Montenegro MCBSM (2006) Construction and evaluation of PVC and sol-gel sensor membranes based on Mn(III)TPP-Cl. Application to valproate determination in pharmaceutical preparations. Anal Bioanal Chem 384:867–875 .
48. Nieto D, Gonzalez-Vadillo AM, Bruña S, Pastor C.J, Ríos-Luci C, Leon LG, Padrón JM, Navarro-Ranninger C, Cuadrado I (2012) Heterometallic platinum(II) compounds with β-aminoethylferrocenes: synthesis, electrochemical behaviour and anticancer activity. Dalton Trans 41: 432−441.
49. Nieto D, Gonzalez-Vadillo AM, Bruña S, Pastor CJ, Kaifer AE, Cuadrado I (2011) Pt(II)-activated coupling of aminoethylferrocene with benzonitrile. A facile access route to a new redox-active bis(ferrocenyl-amidine) anion sensor. Chem Commun 47:10398−10400.
50. Gonsalves KE, Lenz R, Rausch MD (1987) Interfacial polycondensation reactions of the new monomer 1,1′-bis(β -aminoethyl)ferrocene. Appl Organometal Chem 1:81–93.
51. Bucur RV, Bartes A, Mecea V (1978) Kinetic measurements on a stationary disk electrode in a uniformly rotating fluid (SDERF) - I. The limiting diffusion current in the $[Fe(CN)_6]^{3-/4-}$ system. Electrochim Acta 23 (7):641-646.
52. Pochkhidze MS, Asatiani LP, Rukhadze MD, Chitiashvili ZJ, Tsartsidze MA (1999) Determination of ferrocene-A in the blood serum of rabbits using reversed-phase microcolum HPLC. Biomed Chromatogr 13:89-91.

Synergistic effect of MoS_2 and diamond nanoparticles in electrochemical sensors: determination of an anticonvulsant drug

María Dolores Petit-Domínguez[a], Carmen Quintana[a], Luis Vázquez[b], María del Pozo[a], Isabel Cuadrado[c], Ana María Parra-Alfambra[a], Elena Casero[a]

[a]Departamento de Química Analítica y Análisis Instrumental. Facultad de Ciencias. c/ Francisco Tomás y Valiente, Nº7. Campus de Excelencia de la Universidad Autónoma de Madrid. 28049 Madrid. Spain

[b]ESISNA group, Materials Science Factory, Instituto de Ciencia de Materiales de Madrid (CSIC). c/ Sor Juana Inés de la Cruz Nº3. Campus de Excelencia de la Universidad Autónoma de Madrid. 28049 Madrid. Spain

[c]Departamento de Química Inorgánica. Facultad de Ciencias. c/ Francisco Tomás y Valiente, Nº7. Campus de Excelencia de la Universidad Autónoma de Madrid. 28049 Madrid. Spain

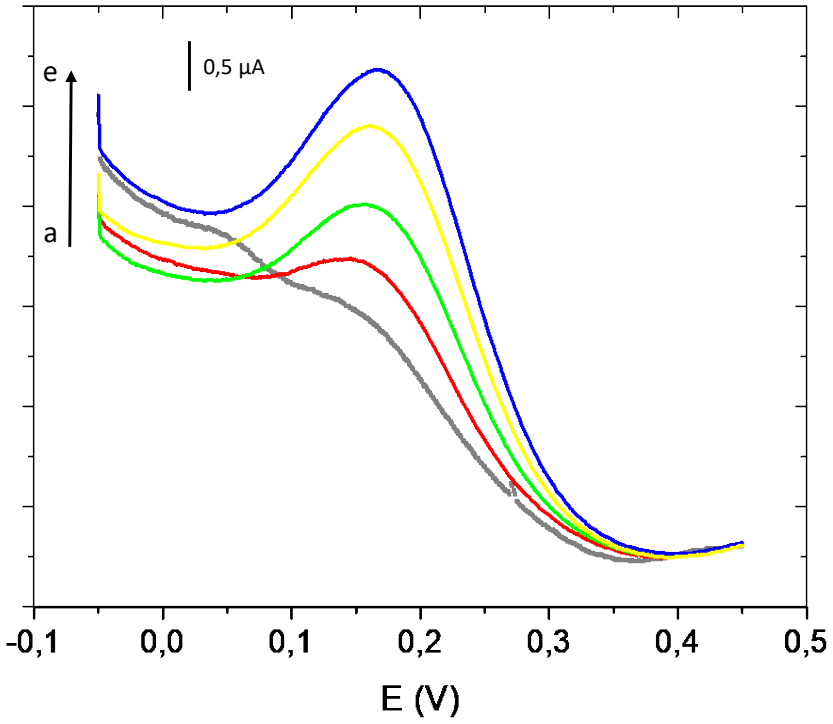

Figure S1. DPVs of GC/MoS_2/DNP sensor in a 0.1 M pH=7.0 phosphate buffer, containing increasing VA-Fc concentration: a) 5.5 10^{-7} M, b) 1.4 10^{-6} M, c) 2.2 10^{-6} M, d) 3.0 10^{-6} M and e) 3.9 10^{-6} M. DPV conditions: range potential from -50 mV to 450 mV, scan rate 10 mV s^{-1}, pulse amplitude 60 mV and step potential 1 mV.

Table S1. Comparison of detection limits of valproic acid obtained by different methods

REFERENCE	METHOD / MATERIALS USED	DERIVATIZATION REAGENT	DETECTION LIMIT (μg/mL)
[35]	GC-MS	----------	1
[36]	LC-MS and CID-MS/MS	----------	0.31
[37]	RP-HPLC	Arylamide N-(2-hydroxyphenyl)-2-propylpentanamide	0.128
[38]	HPLC	2-bromo-2'-acetonaphtone	0.01
[39]	UPLC-MS/MS	2-picolylamine	0.03
[40]	HPLC-UV	2,4'-dibromoacetophenone	5
[41]	HPLC-MS/MS	4-dimethylaminobenzylamine dihydrochloride	0.2
[42]	HS-LPME-GC	----------	0.8
[43]	Capillary electrophoresis	----------	0.08
[44]	Electrochemical sensor (APTES-MNPs/PGE)	----------	0.4
[45]	Nanomechanical biosensor	----------	45
[46]	Proton sensor/Fluorescent detection (TGA-CdTe QDs)	----------	0.24
[47]	Potentiometric sensor- SIA (Mn(III)TPP-Cl/ MTES)	----------	130
Present work	Electrochemical sensor (GC/MoS_2/DNP)	Ferrocene	0.096

GC-MS (gas chromatography-mass spectrometry), LC-MS (liquid chromatography-mass spectrometry), CID-MS/MS (low-energy collision induced dissociation tandem mass spectrometry), RP-HPLC (reversed-phase high performance liquid chromatography), UPLC (ultraperformance liquid chromatography), HPLC-UV (high performance liquid chromatography-ultraviolet), HS-LPME-GC (headspace liquid phase microextraction-gas chromatography), APTES-MNPs (3-aminopropyletriethoxy silane coated magnetic nanoparticles), PGE (pencil graphite surface), TGA-CdTe QDs (thiogycolic acid -capped CdTe quantum dots), SIA (sequential-injection analysis system), Mn(III)TPP-Cl (Manganese (III) tetraphenylporphyrin), MTES (methyltriethoxysilane sol-gel), GC (Glassy carbon electrode), DNP (diamond nanoparticles).